Estimating ecological indicators of karst rocky desertification by linear spectral unmixing method

Xia Zhang [a,*], Kun Shang [a,b], Yi Cen [a], Tong Shuai [a,b], Yanli Sun [a,b]

[a] State Key Laboratory of Remote Sensing Science, Institute of Remote Sensing and Digital Earth, Chinese Academy of Sciences, Beijing 100101, China
[b] University of Chinese Academy of Sciences, Beijing 100049, China

ARTICLE INFO

ABSTRACT

Coverage rates of vegetation and exposed bedrock are two key indicators of karst rocky desertification. In this study, the abundances of vegetation and exposed rock were retrieved from a hyperspectral Hyperion image using linear spectral unmixing method. The results were verified using the spectral indices of karst rocky desertification (KRDSI) and an integrated LAI spectral index: modified chlorophyll absorption ratio index (MCARI2). The abundances showed significant linear correlations with KRDSI and MCARI2. The coefficients of determination (R^2) were 0.93, 0.66, and 0.84 for vegetation, soil, and rock, respectively, indicating that the abundances of vegetation and bedrock can characterize their coverage rates to a certain extent. Finally, the abundances of vegetation and bedrock were graded and integrated to evaluate rocky desertification in a typical karst region. This study suggests that spectral unmixing algorithm and hyperspectral remote sensing imagery can be used to monitor and evaluate karst rocky desertification.

Introduction

Karst is widely distributed and accounts for 12% of the total global land area. It is also one of the most ecologically fragile zones. Karst environments have attracted a great deal of research attention in international geoscience in recent years, particularly in regard to the serious problem of rocky desertification (Wang and Li, 2007). Southwest China, with one of the three largest continuous distributions of karst with exposed carbonate rocks in the world, has experienced severe and rapidly accelerating rocky desertification in the past few decades (Yue et al., 2010, 2013). Owing to its solubility and low acid-insoluble matter content, carbonate forms soil slowly, resulting in a thin soil layer. In addition, disturbances by human activities aggravate soil erosion, forming a unique type of desertification termed "karst rocky desertification."

Research on karst land degradation has mainly relied on ground surveys and statistical data, which limit multi-temporal comparison and multi-scale research. Recently, recognizing the benefits of remote sensing techniques, some researchers have started to employ this approach to monitor and assess karst rocky desertification (Huang and Cai, 2007). However, such methods mostly involve the visual interpretation and computer-assisted digital processing of aerial photographs and satellite images, with high subjectivity and low efficiency. Moreover, multispectral remote sensing images have been mainly used (Hu et al., 2008; Li et al., 2012), and the shortage of spectral information in such images limits the ability to finely discriminate and identify ground objects in karst rocky desertification areas. Because of the lack of spectral information, the vegetation coverage/fraction has been calculated using the dimidiate pixel model. Among linear unmixing models, the simple form of the dimidiate pixel model has been the most extensively used to estimate vegetation coverage and monitor dynamic changes in vegetation on a large scale (Cui, 2010; Zeng et al., 2000; Xiao and Moody, 2005). This model assumes that a pixel consists of two components, vegetation and soil, but ignores the type of vegetation (Xiao and Moody, 2005; Liang et al., 2012). It also does not account for rocks, which are distributed widely in karst rocky desertification regions.

As key ecological indicators, coverage rates of vegetation and bedrock are usually used to characterize the surface symptoms, extent, and degree of karst rocky desertification. Hyperspectral remote sensing imagery, composed of hundreds of continuous narrow bands obtained by imaging spectrometry, allows us to characterize the coverage rates of land cover in two ways. The first is to solve a spectrum mixture model and obtain the abundance of each component in each pixel with high accuracy. The abundance could represent the coverage rate. The second is to develop a spectral index sensitive to the coverage rate. However, only a few previous studies have attempted to develop spectral indices to characterize the coverage rate of vegetation, soil, and rock in karst rocky

* Corresponding author. Tel.: +86 10 64806206; fax: +86 10 64806206.
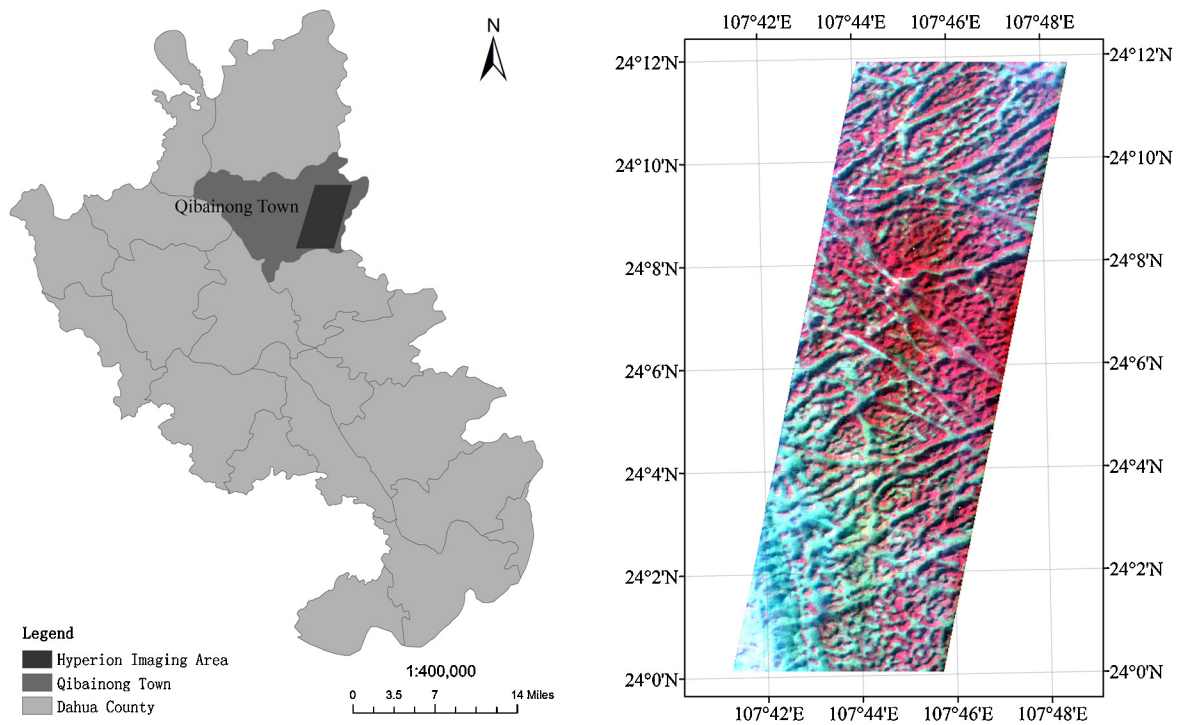*E-mail address:* zhangxia@radi.ac.cn (X. Zhang).

Fig. 1. Sketch map of locations of study site and Hyperion imaging area. The dark parallelogram in the left map indicates the location of the Hyperion imging area on the right.

desertification environments (Yue et al., 2010, 2013; Ding et al., 2011), and most were based on hyperspectral data obtained in the field.

This study explored the application of linear spectral unmixing method using hyperspectral remote sensing data for the purpose of retrieving the coverage rates of rock and vegetation in typical karst rocky desertification areas. First, newly developed spectral indices were verified using field data for their ability to characterize the coverage rates of the typical land covers. Then the best indices were applied to hyperspectral remotely sensed images, and the correlations were analyzed between the abundance retrieved by spectral unmixing and by the image-based spectral indices. Finally, the coverage rates for rock and vegetation, represented by abundances, were classified and integrated to obtain a rocky desertification evaluation map. We present the results and discuss their implication in the conclusions.

Study site and data sets

Study site

The study site was Qibainong Town, a typical limestone karst rocky desertification area (see Fig. 1). Qibainong Town is located in Dahua County, Guangxi Province, China, and has the most completely preserved karst landforms in the world. The town covers an area of 203 km² and includes more than 5000 hills rising 800–1000 m above the sea level and more than 1300 depressions. The most obvious land surface symptoms are the widespread exposure of carbonate rocks and low vegetation cover. Soil erosion is serious as a result of human disturbance and natural factors. Conifer forest, broadleaf forest, mixed forest and shrubs mainly grow on the hills with thicker soil layer. The soil in valley alluvial zone is fertile and suitable for farming, but the area is extremely limited. Moreover, the variety of complex terrain increases spatially landscape heterogeneity, which appears as discontinuously distributed soil

rock, and fragmented ecological spaces for vegetation. Land covers here are often mixtures of several types.

Hyperspectral remote sensing imagery

This study used an EO-1 Hyperion hyperspectral image acquired on 3 March 2008 in clear atmospheric conditions. The image, obtained from the US Geological Survey (USGS), has 242 bands in the 400–2500 nm spectral range at a spectral resolution of 10 nm and spatial resolution of 30 m. The data product is level 1R with radiometric calibration but without geometric correction. As the swath width of the Hyperion image was only 7.5 km, it covered only about 25% of the total area of Qibainong Town. The imaging area was in the west of the town (see Fig. 1).

Data preprocessing was performed on the Hyperion data, including band selection, atmospheric correction, smile effect correction, and geometric correction. Regarding band selection, 44 bands without radiometric calibration (i.e., bands 1–7, 58–76, 225–242) were removed. In addition, bands 77–78 (which repeated bands 56–57) were removed, as were 20 bands severely contaminated by water vapor. The remaining 176 bands were used for further processing and analysis. Atmospheric correction was performed using ACORN software and a reflectance image was obtained. The smile effect was corrected by using a column mean adjusted method in minimum noise fraction (MNF) space (Goodenough et al., 2003). With reference to Landsat Thematic Mapper (TM) imagery, a geometric correction was applied to the Hyperion image to obtain accuracy within 0.5-pixel root mean-square error (RMSE).

Field experiment data

A field experiment was carried out at the study site in November 2010 to obtain reflectance spectra and coverage rate data for complex ground objects that corresponded to the degree of karst rocky desertification. In total, 132 samples (ground objects) were selected

for measurement. Each sample contained different proportions of vegetation, soil, and rock. For each sample, the spectrum was measured using an analytical spectral device (ASD) FieldSpecFR spectrometer with a black colored square frame placed to mark the area observed. The side length of the square frame was 66 cm. The spectrometer was held 1.5 m above the surface with a field of view of 25°, and hence the observed area corresponded to a circle with a radius of 33 cm. A digital camera at the same height photographed this area simultaneously. This guaranteed that the area observed using the ASD corresponded exactly to the inscribed circle of the square frame area photographed by the digital camera.

The digital photos were then clipped so that the inscribed circles of the square fame corresponded to the areas observed by the ASD, and these were then classified into three types (i.e., vegetation, soil and rock) using the maximum likelihood classification routine in ENVI software. Then, the number of pixels of each type was divided by the total number of pixels in the circle to obtain the coverage rate. In this manner, coverage rates of each sample were obtained. In total, 132 sets of spectra and coverage rates were obtained and used to validate the spectral indices of karst rocky desertification.

Methods

Spectral indices of karst rocky desertification

Spectral indices of karst rocky desertification (KRDSI) were first developed by Yue et al. (2010). Karst bedrock is mostly composed of carbonate, and thus the spectral feature of the carbonate ion around 2300 nm characterizes the KRDSI for rock. The spectral feature of clay around 2200 nm characterizes the KRDSI for soil, as the soil in karst environments is dominated by limestone with high clay content. The KRDSIs were expressed as follows:

$$KRDSI_1 = 2\rho_c - (\rho_a + \rho_b) \tag{1}$$

$$KRDSI_2 = \frac{2\rho_c}{\rho_a + \rho_b} \tag{2}$$

$$KRDSI_3 = \frac{\rho_a - \rho_c}{\rho_a + \rho_c} \tag{3}$$

$$KRDSI_4 = \rho_c - \rho_0 \tag{4}$$

where ρ is the spectral reflectance; a, b, and c represent the wavelengths (nm) of the two shoulders and peak of absorption, respectively; and ρ_0 is the estimated reflectance at wavelength c, assuming there are no absorption features present and therefore interpolating linearly between reflectances at wavelengths a and b.

For vegetation, three typical spectral indices were selected: the area of red edge (ARG), normalized difference vegetation index (NDVI), and modified chlorophyll absorption ratio index (MCARI2). Among them, ARG and MCARI2 are the unique hyperspectral remote sensing vegetation indices.

The red edge was defined as the wavelength where the maximum of the first derivative occurred in the spectral range of 680–750 nm. Several studies have shown that measures based on the red edge position or shape are likewise well correlated with biophysical parameters at the canopy level, but less sensitive to spectral noise caused by the soil background and by atmospheric effects (Miller et al., 1985; Baret et al., 1992; Yumako et al., 2012). In this study, one feature of the red edge, ARG, was analyzed. ARG was defined as the integral of the reflectance spectra vs. wavelength within the spectral range of 680–750 nm, given as follows:

$$ARG = \int_{680}^{750} R_\lambda \, d\lambda \tag{5}$$

where R_λ is the reflectance at wavelength λ.

In general, ARG is determined using a derivative method (Chen and Elvidge, 1993). However, direct derivative processing of the original image spectra tended to magnify local noise. Since it has been proved that the spectrum within the 680–800 nm range can be fitted almost perfectly using the inverse-Gauss function (Miller et al., 1990), the inverse-Gauss fit was utilized on the original spectra, and the derivative was then computed to obtain the ARG.

As an improved version of modified chlorophyll absorption ratio index (MCARI) (Daughtry et al., 2000), MCARI2 was developed by Haboudane et al. (2004), which integrated a near-infrared wavelength to increase the sensitivity to LAI changes and incorporated a soil adjustment factor to reduce soil contamination effects. It was proved to be the better predictor of green LAI than the existing vegetation indices. MCARI2 can be calculated by the following formula:

$$MCARI2 = \frac{1.5[2.5(\rho_{700} - \rho_{670}) - 1.3(\rho_{700} - \rho_{550})]}{\sqrt{(2\rho_{700} + 1)^2 - (6\rho_{700} - 5\sqrt{\rho_{670}}) - 0.5}} \tag{6}$$

where ρ_{700}, ρ_{670}, and ρ_{550} represent the reflectance of wavebands centered around 700, 670, and 550 nm, respectively (the same applies below).

NDVI is the most well-known vegetation index, which is based on the contrast between the maximum absorption in the red due to chlorophyll pigments and the maximum reflection in the infrared caused by leaf cellular structure. It has the advantage of enhancing the contrast between soil and vegetation while minimizing the effects of illumination conditions. Moreover, it has the nearly simplest expression among the various ratio indices. It has been widely used to estimate LAI and vegetation coverage (Cohen et al., 2003a; Yue et al., 2013). Narrow-band version of NDVI is mostly calculated from the 670 (red) and 800 nm (NIR) spectral bands of hyperspectral remote sensing data (Broge and Leblanc, 2000; Haboudane et al., 2004). In this study, narrow-band NDVI was calculated as

$$NDVI = \frac{\rho_{800} - \rho_{670}}{\rho_{800} + \rho_{670}} \tag{7}$$

Spectral unmixing and abundance retrieval

Because bedrock, vegetation, and soil are land covers typical of rocky desertification, we determined vegetation, soil, and rock as endmembers. An endmember selection algorithm was adopted to chose the three endmembers. Then, linear spectral unmixing method was employed to retrieve the abundance. The spectral unmixing and abundance retrieval was implemented in three steps: MNF transformation, endmember extraction, and linear spectral unmixing.

MNF transformation

A minimum noise fraction (MNF) transformation was applied to the Hyperion image for reducing dimensions and denoising. The advantage of MNF over principal component analysis (PCA) is that it accounts for the fact that the noise in some bands may be larger than the signal in other bands (Boardman and Kruse, 1994). MNF can transform images with decreasing image quality with increasing component number.

Endmember selection

Because of the high landscape heterogeneity of karst environments, mixed pixels are very common. The conventional image-based endmember selection approach based on scatterplots of the image bands may not be effective in identifying a sufficient number of endmembers. In this paper, we employed the sequential maximum angle convex cone (SMACC) algorithm to identify spectral image endmembers. The extreme points were used to determine a convex cone, which defined the first endmember. A
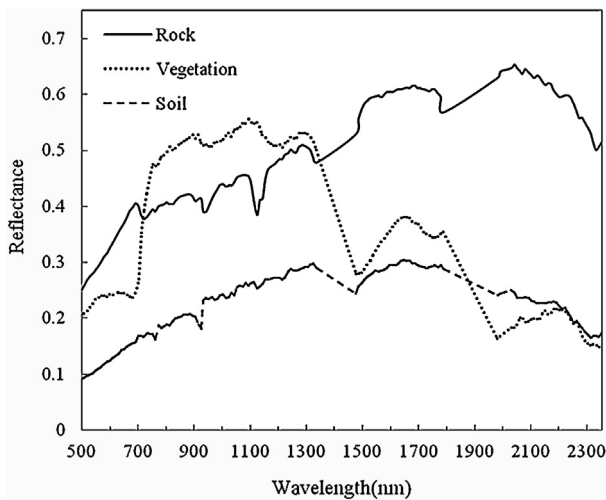
Fig. 2. Representative endmembers of vegetation, soil, and rock extracted by SMACC.

Table 1
Linear regression of spectral indices and coverage rates obtained from field experiment data.

	Spectral index	Linear regression equation	R^2
Soil	KRDSI$_1$-soil	$y = -11.502x + 8.0863$	0.7047
	KRDSI$_2$-soil	$y = -0.3588x + 1.233$	0.6113
	KRDSI$_3$-soil	$y = 0.1811x - 0.0839$	0.5868
	KRDSI$_4$-soil	$y = 5.7511x - 4.0431$	0.7652
Rock	KRDSI$_1$-rock	$y = -6.9207x - 2.1327$	0.28
	KRDSI$_2$-rock	$y = 0.008x + 0.902$	0.0005
	KRDSI$_3$-rock	$y = -0.1846x + 0.1448$	0.2212
	KRDSI$_4$-rock	$y = 6.2857x - 0.943$	0.5103
Vegetation	ARG	$y = 37.914x + 4.642$	0.78
	NDVI	$y = 0.9095x + 0.2637$	0.7671
	MCARI2	$y = 1.255x + 0.216$	0.8285

constrained oblique projection was applied to the existing cone to derive the next endmember. The cone was then increased to include a new endmember. This process was repeated until a projection derived an endmember that already existed within the convex cone, or until a specified number of endmembers was satisfied (Gruninger et al., 2004).

In this study, SMACC was executed by IDL language programming. When implemented SMACC, the output endmember number was set as 5, 10 and 15 respectively. Better endmembers for rock, soil and vegetation could be identified easily from 10-endmember-output. So by matching with the field-measured spectra, one typical endmember was then selected for each ground object from the 10-endmember-output. The representative endmembers for three typical ground objects (i.e., vegetation, soil, and rock) were shown in Fig. 2. The pairwise correlation coefficients (R^2) among the three endmembers were 0.1014 for rock and vegetation, 0.4528 for rock and soil, 0.1698 for vegetation and soil. All correlation coefficients were much lower than 0.6. According to Meer and Jia (2012), when the correlation exceeds 0.6 (identified as a critical level), the inversion though a linear spectral unmixing becomes prone to error. Thus, in this study the selected three endmembers with low correlations could ensure to some extent the inversion by linear spectral unmixing was stable and less sensitive to error.

Linear spectral unmixing

The linear spectral unmixing (LSU) approach was adopted to calculate the abundance of endmembers for each pixel. LSU assumes that the spectrum measured by a sensor is a linear combination of the spectra of all components (endmembers) within the pixel, and the spectral proportions of the endmembers (i.e., their abundance) reflect the proportion of area covered by distinct features on the ground (Adams et al., 1995). The general equation for linear spectral mixing can be expressed as

$$R_{ij,\lambda} = \sum_{n=1}^{N} f_{ij,n} R_{n,\lambda} + E_\lambda \tag{8}$$

where $R_{ij,\lambda}$ is the measured reflectance at wavelength λ for pixel ij, where i is the column pixel number and j is the line pixel number; $f_{ij,n}$ is the fraction of endmembers n contributing to the image spectrum of pixel ij; N is the total number of endmembers; $R_{n,\lambda}$ is the reflectance of endmember n at wavelength λ; and E_λ is the error at wavelength λ of the fit of N spectral endmembers.

The fraction $f_{ij,n}$ can be solved using a least-square method with fully constrained or partial constraints unmixing. Fully constrained

unmixing means that the sum of the endmember fractional (abundance) values for each pixel must equal unity, which requires a complete set of endmembers. Therefore, it should meet the following two conditions:

$$0 \le f_{ij,n} \le 1 \tag{9}$$

$$\sum_{n=1}^{N} f_{ij,n} = 1 \tag{10}$$

In the majority of cases, the unmixing is only partially constrained because the extracted endmember set is incomplete for the image and only term (9) (i.e. Eq. (9)) is satisfied.

In this study, fully constrained linear unmixing and partially constrained unmixing were both applied to the Hyperion image to obtain and compare the best-fit abundance result.

Results and analysis

Validation of KRDSI with field data

KRDSI values for soil and rock were calculated from the field spectra according to the four KRDSI expressions shown in Section "Spectral indices of karst rocky desertification". For vegetation, three current spectral indices were calculated from the field spectra. The corresponding coverage rates were estimated by classifying the digital photographs within the viewing field of the ASD. The correlations between the spectral indices and coverage rates were then obtained and are shown in Table 1.

Table 1 shows that all four forms of KRDSI have a significant linear relationship with the coverage rate of soil, with R^2 reaching 0.76, indicating that the spectral absorption feature around 2200 nm was effective in characterizing soil features (i.e., clay) in the karst environment. However, only the fourth form of KRDSI had a significant linear correlation with the coverage rate for rock, and the other three forms were weak or demonstrated no correlation with the rock coverage rate. Even though carbonate is the dominant rock in karst environments, dolomite can also be present, and as dolomite content increases, the spectral absorption center shifts to shorter wavelengths. In addition, the differing extent of erosion of carbonate rocks also affects the absorption features. Thus, it is difficult to characterize the absorption features of rock using spectral indices. However, among the four forms, the fourth form of KRDSI was able to characterize the coverage rate of rock to a certain extent, with an R^2 value of 0.5103.

For the vegetation coverage rate, MCARI2 performed better than did ARG or NDVI, due to its sensitivity to the canopy effect and less sensitivity to soil background. Therefore, MCARI2, KRDSI$_4$-rock, and KRDSI$_4$-soil were selected as the best indicators to verify the
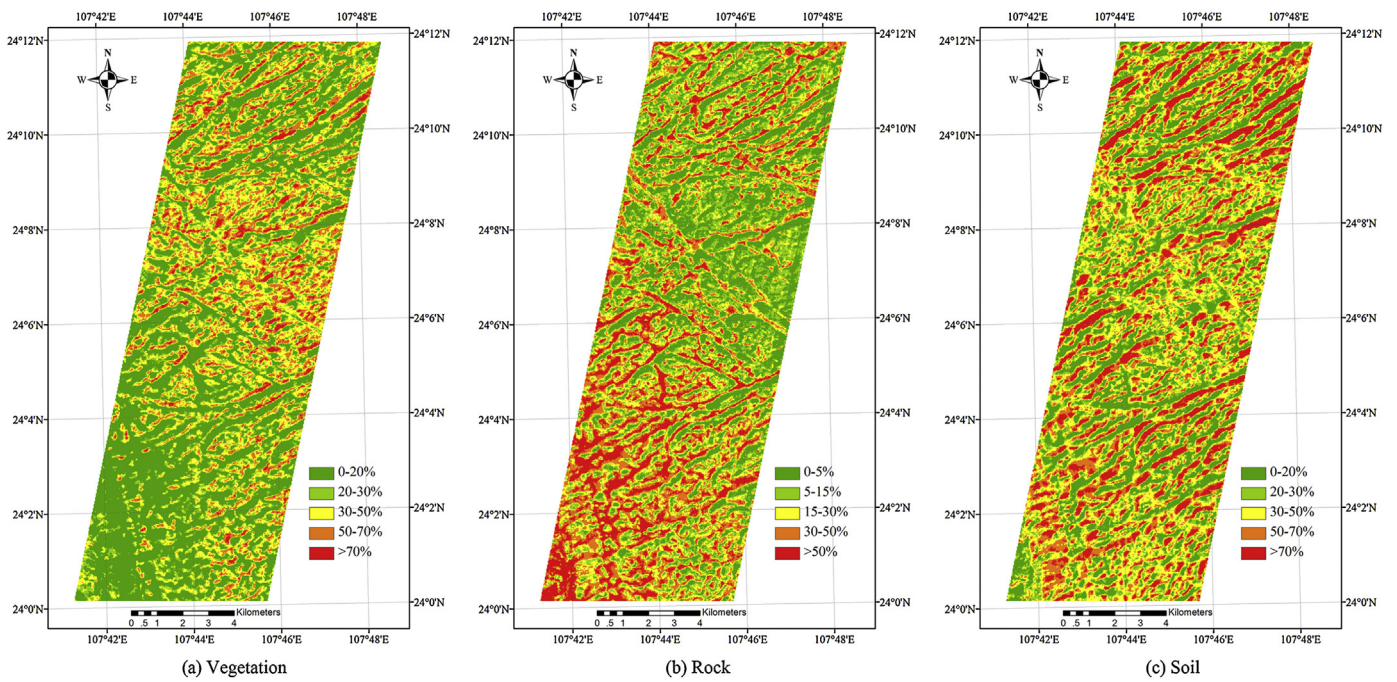
Fig. 3. Abundance maps retrieved using a partially constrained linear unmixing algorithm.

abundances retrieved using the linear spectral unmixing method and hyperspectral remote sensing imagery.

Abundance map and its correlation with image-based spectral indices

Fig. 3 shows the abundances of vegetation, soil, and rock retrieved from the Hyperion image using the partially constrained linear unmixing algorithm. The RMSE is shown in Fig. 4. Fig. 5 shows

the abundance using a fully constrained linear unmixing algorithm and Fig. 6 shows the corresponding RMSE.

RMSE was chosen as the error indicator for the abundance result. A smaller RMSE means better accuracy of the abundance maps. Most RMSE values were lower than 0.03 for both the fully constrained and partially constrained results. However, the RMSE for fully constrained unmixing was slightly higher than that for partially constrained unmixing; this may be because only three endmembers were chosen in this study and
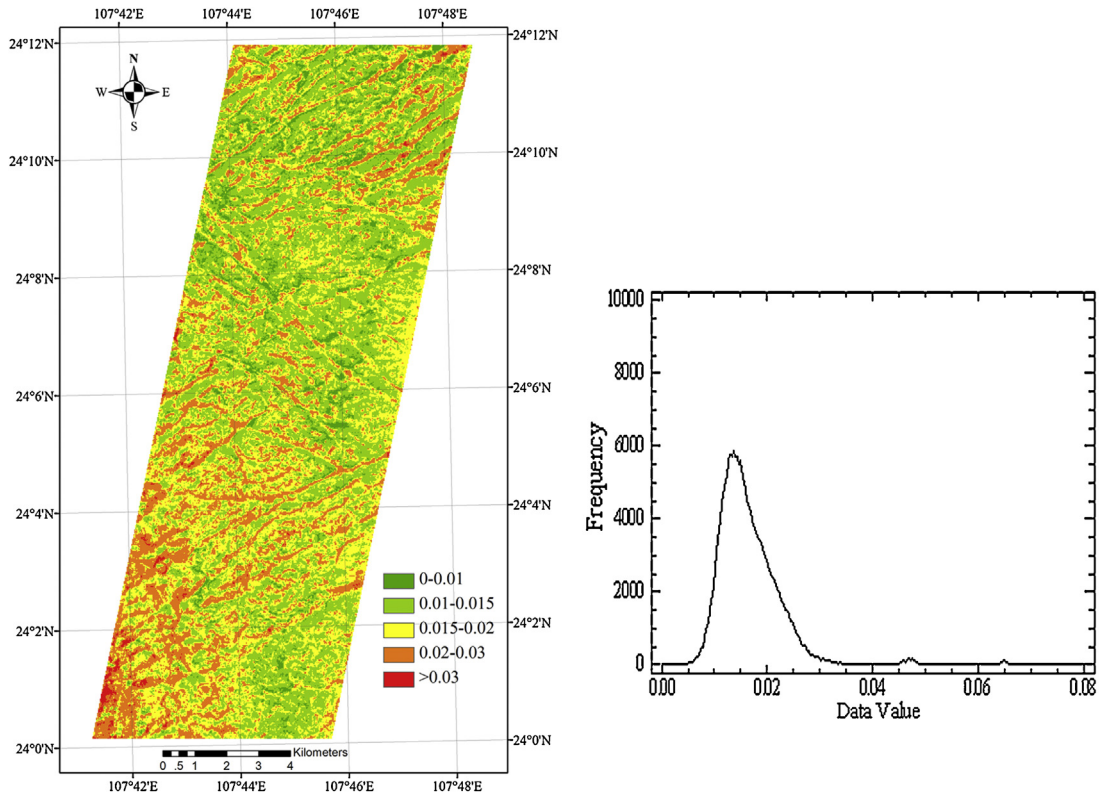

Fig. 4. RMSE map and the corresponding histogram for results obtained using partially constrained linear unmixing.
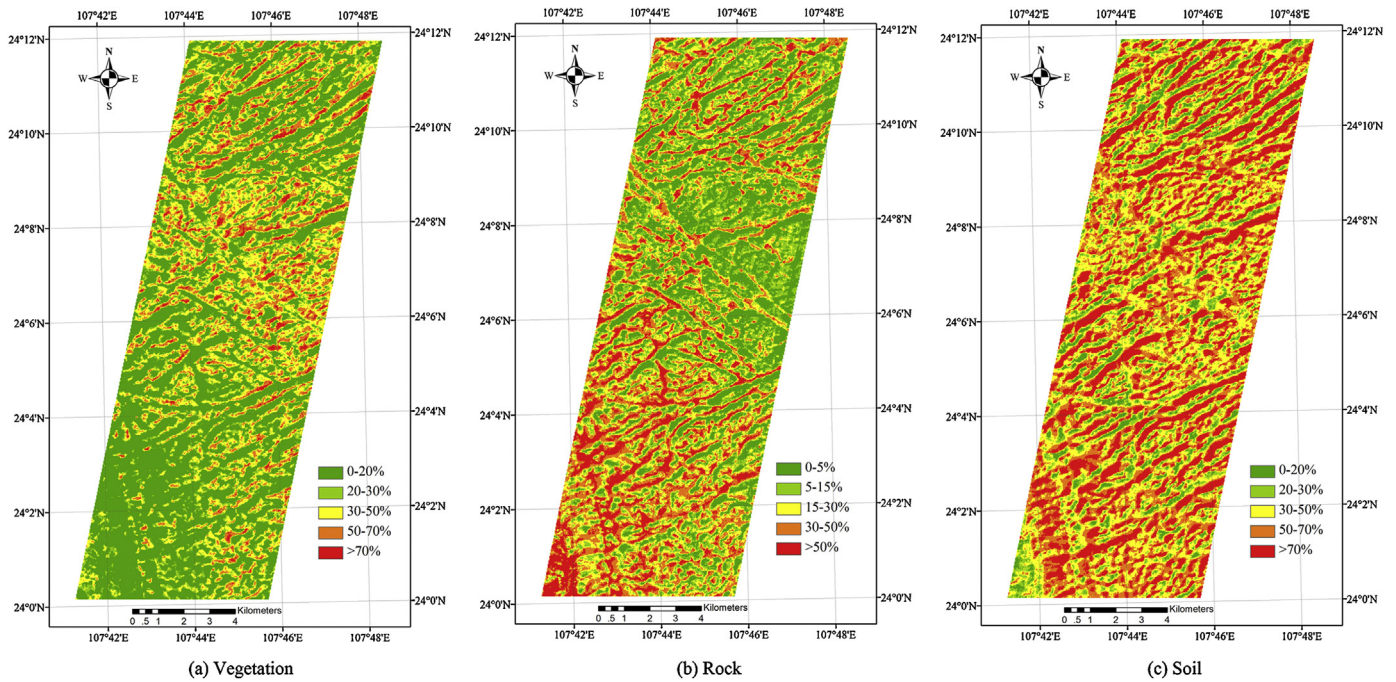
Fig. 5. Abundance maps retrieved using a fully constrained linear unmixing algorithm.

the endmember set may be incomplete, meaning that the condition that the terms sum to unity was not satisfied (Liu et al., 2008). In addition, the abundance distribution was fairly consistent for the two constrained unmixing results, except for soil which had obviously lower values for fully constrained unmixing than for partially constrained, while the latter was more consistent with the coverage rate distribution characterized by the spectral indices.

Therefore, the partially constrained result was considered more reliable and was used to analyze the correlation with the spectral indices.

Considering the results presented in Section "Validation of KRDSI with field data", MCARI2 as well as $KRDSI_4$-rock and $KRDSI_4$-soil were applied to the Hyperion image data. On the basis of the spectral feature analysis of image spectra, meanwhile
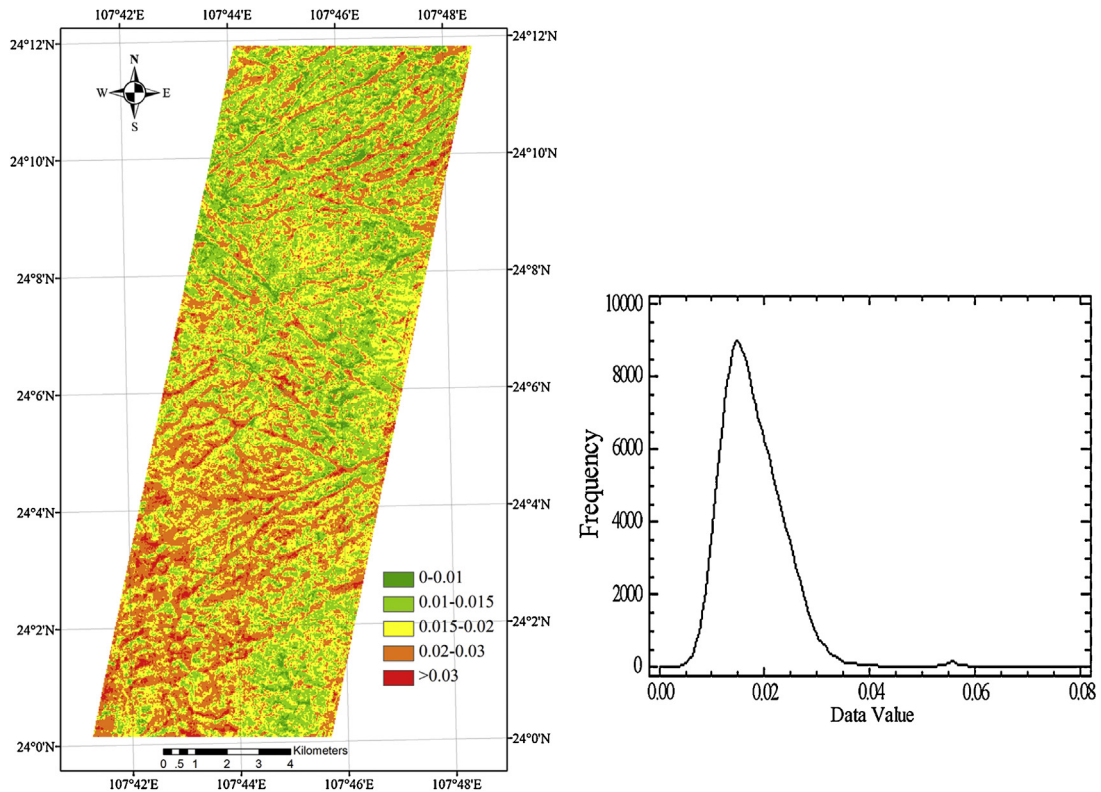

Fig. 6. RMSE map and the corresponding histogram for results obtained using fully constrained linear unmixing.
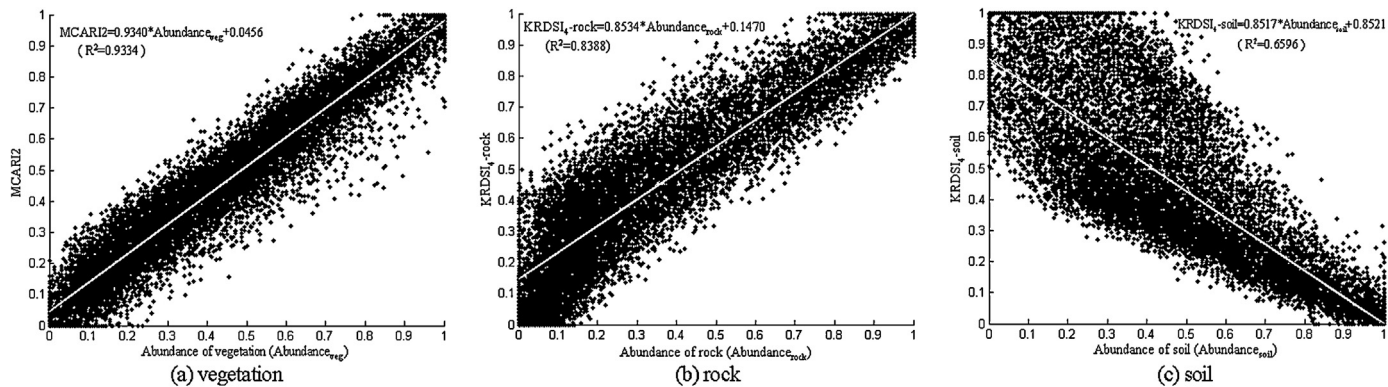
Fig. 7. Linear regression analysis between the spectral index images and the corresponding abundance images.

considering the selected bands must have higher SNR, a, b, and c were determined to be 2209.6, 2387.5, and 2340 nm for rock and 2101.7, 2347.2, and 2207.1 nm for soil, respectively.

The correlation between the spectral index images and the abundance image was analyzed. Fig. 7 shows the scatter diagrams and the statistical correlation results. The R^2 values were 0.93, 0.66, and 0.84 for vegetation, soil, and rock, respectively, indicating that both the proposed soil and rock spectral indices and MCARI2 can be used to characterize the fractional coverage of the corresponding land cover effectively.
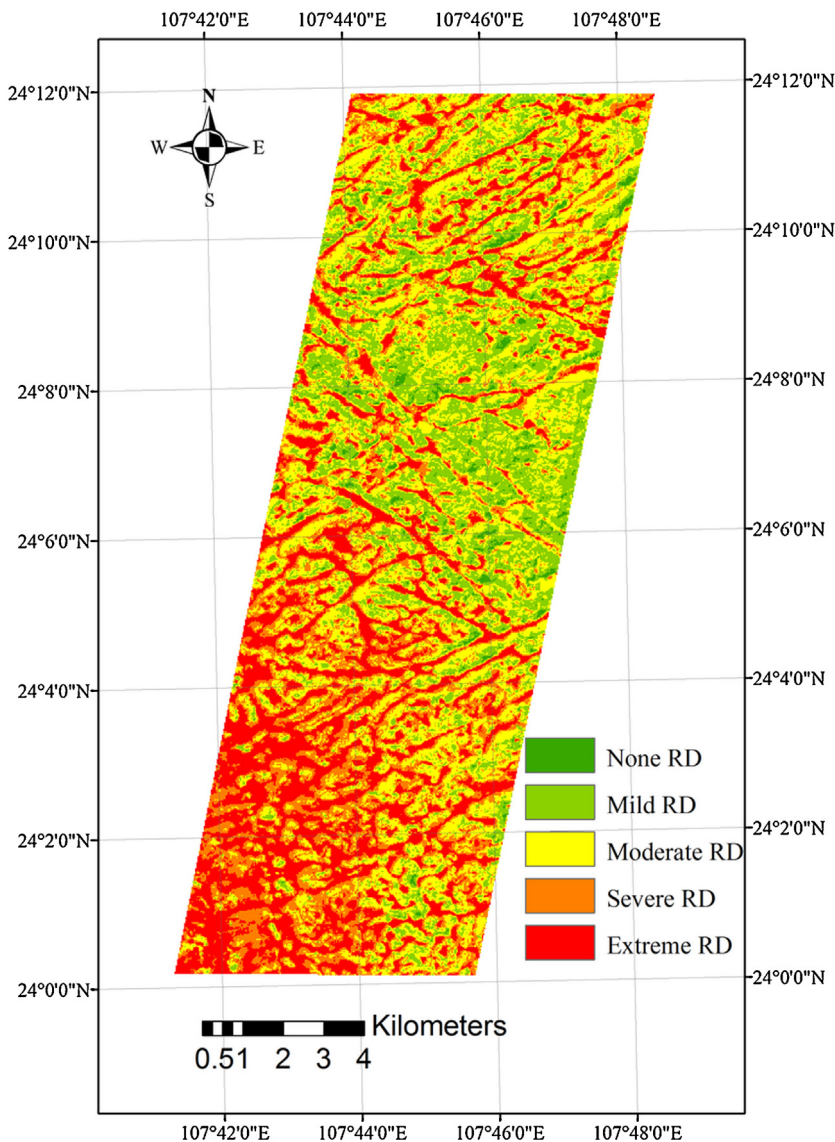

Fig. 8. Map of the degree of rocky desertification in the study area.

Table 2
Rocky desertification evaluation index system.

	No RD[a]	Slight RD	Moderate RD	Severe RD	Extreme RD
Vegetation	>70%	50–70%	30–50%	20–30%	<20%
Rock	<5%	5–15%	15–30%	30–50%	>50%
Classification and assignment	1	2	3	4	5
Classification rule	1	2–4	4–9	9–16	16–25

[a] RD, rocky desertification.

Table 3
Area and percentage of rocky desertification (RD).

RD degree	Area (km^2)	Proportion of total area (%)
No RD	2.2887	1.41
Slight RD	31.2381	19.24
Moderate RD	52.4763	32.32
Severe RD	38.0232	23.42
Extreme RD	38.3598	23.62

Evaluation of the degree of rocky desertification

Referring to the specifications of the State Environmental Protection Administration of China in regard to evaluation of sensitivity to rocky desertification (Huang and Cai, 2007), we selected the abundances of rock and vegetation as the key indicators and classified them (see Table 2). The classified indicators were then multiplied by each other and were classified into five degrees of rocky desertification according to the last row of Table 2.

The degree of rocky desertification is mapped in Fig. 8. Severe and extreme RD is mainly distributed in the south and southwest of our study area, which agrees with our ground-truth data. The north-central part showed mainly slight and moderate RD, with a small amount of extreme RD. In the northern part, more extreme RD was distributed, while the other four RD degrees were mixed. For each RD degree, the area percentage was calculated by dividing the pixel number of this RD degree by the total pixel number of the imaging area. The area statistics indicate (see Table 3) that extreme, severe, moderate, slight, and no RDs accounted for 23.6%, 23.4%, 32.3%, 19.2%, and 1.4% of the total study area, respectively, which verified that severe RD was distributed widely in Qibainong Town. Urgent counteractive measures are thus needed in this area. However, as the imaging area of the Hyperion image covered only about 25% of the total area of Qibainong Town, and the official statistics data is on the basis of town unit, the area percentages were not able to be validated with the official statistics data in this study. With the development of hyperspectral sensor and associated technologies, we hope to acquire hyperspectral image with wide enough swath to completely validate our method and results in the near future.

Conclusions

Rocky desertification (RD) is one of the most serious environmental problems in karst regions in southwest China. The fractional covers of vegetation and exposed bedrock are the main indicators of karst RD. Hyperspectral remotely sensed images contain hundreds of continuous narrow bands and are useful for assessing land cover and the key RD indicators at a pixel scale.

In this study, first, newly developed spectral indices for rocky desertification (KRDSI) were verified by correlation analysis with coverage rates determined from field data. Significant linear correlations were obtained for KRDSI$_4$-soil and KRDSI$_4$-rock, with coefficients of determination (R^2) of 0.76 and 0.51, respectively. The vegetation chlorophyll index MCARI2 had the highest R^2 (0.83) among the red edge indices and other vegetation indices. Therefore, KRDSI$_4$-soil, KRDSI$_4$-rock, and MCARI2 were applied to the hyperspectral remotely sensed imagery to obtain maps of coverage rates.

Second, a hyperspectral Hyperion image was obtained and the abundances of soil, rock, and vegetation were retrieved using a spectral unmixing method. The method was implemented in three steps: a minimum noise fraction (MNF) transformation was applied to reduce the noise and dimension, automatic endmember extraction was applied using a sequential maximum angle convex cone (SMACC) algorithm, and finally linear spectral unmixing using a fully constrained unmixing and a partially constrained unmixing algorithm was performed. The fully constrained result had a slightly larger RMSE than the partially constrained unmixing result, which may be because the three endmembers chosen in this study were an incomplete endmember set over the imaging area, and thus the constraint of terms summing to unity was not satisfied. The partially constrained result was therefore considered to be more reliable for this study and was used to analyze the correlation with the spectral indices. The abundances of the three typical land covers had significant linear correlations with the two non-vegetation spectral indices and MCARI2. The R^2 values of 0.93, 0.66, and 0.84 for vegetation, soil, and rock, respectively, indicated that abundances retrieved using a partial linear unmixing algorithm could characterize the fractional coverage of the corresponding land covers effectively.

Finally using the coverage rates of rock and vegetation characterized by their abundance as key indicators of rocky desertification, we mapped RD by classifying and assigning the two indicators and integrating them over the study area. The RD classification/evaluation map was consistent with the ground-truth data.

Our research shows the potential for monitoring and evaluating karst RD using hyperspectral remote sensing data and linear spectral unmixing method. However, several improvements are still necessary. The first is to develop an endmember-variable pixel unmixing approach to overcome the high landscape heterogeneity of karst environments. For this purpose, a spectral library of typical karst ground objects should be established. Moreover, topographic correction should be emphasized since complex topography in karst region increases landscape heterogeneity. The second improvement needed is a way to combine the spectral index with abundance retrieved by spectral unmixing method to improve the accuracy of coverage rates. Finally, coverage rate data should be acquired in field experiments to allow matching to the pixel size of remotely sensed images.

Acknowledgements

References

Adams, J.B., Sabol, D.E., Kapos, V., et al., 1995. Classification of multispectral images based on fractions of endmembers: application to land-cover change in the Brazilian Amazon. Remote Sens. Environ. 52, 137–154.

Baret, F., Jacquemoud, S., Guyot, G., Leprieur, C., 1992. Modelled analysis of the biophysical nature of spectral shifts and comparison with information content of broad bands. Remote Sens. Environ. 41, 133–142.

Boardman, J.W., Kruse, F.A., 1994. Automated spectral analysis: a geological example using AVIRIS data, north Grapevine Mountains. In: Proceedings of ERIM Tenth Thematic Conference on Geologic Remote Sensing, pp. I-407–I-418.

Broge, N.H., Leblanc, E., 2000. Comparing prediction power and stability of broadband and hyperspectral vegetation indices for estimation of green leaf area index and canopy chlorophyll density. Remote Sens. Environ. 76, 156–172.

Chen, Z., Elvidge, C.D., 1993. Description of derivative-based high spectral-resolution (AVIRIS) green vegetation index. Proc. SPIE 1937, 43–54.

Cohen, W.B., Maierpserger, T.K., Gower, S.T., Turner, D.P., 2003a. An improved strategy for regression of biophysical variables and Landsat ETM+ data. Remote Sens. Environ. 84, 561–571.

Cui, Y., 2010. Extraction of vegetation fraction based on the dimidiate pixel model and vegetation index transform plan. Proc. SPIE 7752 (1), 775202-1–775202-8.

Daughtry, C.S.T., Walthall, C.L., Kim, M.S., et al., 2000. Estimating corn leaf chlorophyll concentration from leaf and canopy reflectance. Remote Sens. Environ. 74, 229–239.

Ding, L., Zhang, X., Ji, M., Shuai, T., 2011. Spectral indices for estimating the fractional cover of non-vegetation land-cover types in karst environment. In: International Conference on Remote Sensing, Environment and Transportation Engineering, pp. 2499–2502.

Goodenough, D.G., Dyk, A., Niemann, K.O., et al., 2003. Processing Hyperion and ALI for forest classification. IEEE Trans. Geosci. Remote Sens. 41 (6), 1321–1331.

Gruninger, J., Ratkowski, A.J., Hoke, M.L., 2004. The sequential maximum angle convex cone (SMACC) endmember model. Proc. SPIE 5425, 3885–3895.

Haboudane, D., Miller, J.R., Pattey, E., et al., 2004. Hyperspectral vegetation indices and novel algorithms for predicting green LAI of crop canopies: modeling and validation in the context of precision agriculture. Remote Sens. Environ. 90, 337–352.

Hu, J., Xiong, K., An, Y., 2008. The application of CBERS-02 image in remote sensing interpretation for karst rock desertification with a special reference of Qiannan prefecture, Guizhou province. J. Guizhou Normal Univ. (Nat. Sci.) 26 (2), 39–42.

Huang, Q.H., Cai, Y.L., 2007. Spatial pattern of karst rock desertification in the middle of Guizhou province, Southwestern China. Environ. Geol. 52, 1325–1330.

Li, S., An, Y., Hua, H., 2012. Automated method based on change detection for extracting karst rocky desertification information using remote sensing. Remote Sens. Technol. Appl. 27 (1), 149–153.

Liang, S., Li, X., Wang, J., 2012. Advanced Remote Sensing: Terrestrial Information Extraction and Applications. Academic Press.

Liu, J., Miller, J.R., Haboudane, D., Pattey, E., Hochheim, K., 2008. Crop fraction estimation from CASI hyperspectral data using linear spectral unmixing and vegetation indices. Can. J. Remote Sens. 34 (S1), S124–S138.

Meer, V.F.D., Jia, X., 2012. Collinearity and orthogonality of endmembers in linear spectral unmixing. Int. J. App. Earth Observ. Geoinf. 18, 491–503.

Miller, J.R., Hare, E.W., Neville, R.A., et al., 1985. Correlation of metal concentrations with anomalies in narrow band multispectral imagery of the vegetation red reflectance edge. In: Proceedings of the International Symposium on Remote Sensing, Fourth Thematic Conference, Remote Sensing for Exploration Geology, pp. 143–153.

Miller, J.R., Hare, E.W., Wu, J., 1990. Quantitative characterization of the vegetation red edge reflectance 1. An inverted-Gaussian reflectance model. Int. J. Remote Sens. 11 (10), 1755–1773.

Wang, S., Li, Y., 2007. Problems and development trends about researches on karst rocky desertification. Adv. Earth Sci. 22, 474–485.

Xiao, J., Moody, A., 2005. A comparison of methods for estimating fractional green vegetation cover within a desert-to-upland transition zone in central New Mexico, USA. Remote Sens. Environ. 98, 237–250.

Yue, Y., Wang, K., Liu, B., et al., 2013. Development of new remote sensing methods for mapping green vegetation and exposed bedrock fractions within heterogeneous landscapes. Int. J. Remote Sens. 34 (14), 5135–5136.

Yue, Y., Zhang, B., Wang, K., et al., 2010. Spectral indices for estimating ecological indicators of karst rocky desertification. Int. J. Remote Sens. 31 (8), 2115–2122.

Yumako, K., William, R., John, S., et al., 2012. Red edge as a potential index for detecting differences in plant nitrogen status in winter wheat. J. Plant Nutr. 35 (10), 1526–1541.

Zeng, X., Dickinson, R.E., Walker, A., Shaikh, M., et al., 2000. Derivation and evaluation of global 1-km fractional vegetation cover data for land modeling. J. Appl. Meteorol. Climatol. 39, 826–839.